A Search for Neutrinos from the Solar *hep* Reaction and the Diffuse Supernova Neutrino Background with the Sudbury Neutrino Observatory

B. Aharmim[5], S.N. Ahmed[13], A.E. Anthony[17], E.W. Beier[12], A. Bellerive[3], M. Bergevin[6,4], S.D. Biller[11], M.G. Boulay[13,7], Y.D. Chan[6], M. Chen[13], X. Chen[6,19], B.T. Cleveland[11], G.A. Cox[15], C.A. Currat[6], X. Dai[13,11], F. Dalnoki-Veress[3,20], H. Deng[12], J. Detwiler[15], M. DiMarco[13], P.J. Doe[15], G. Doucas[11], P.-L. Drouin[3], F.A. Duncan[16,13], M. Dunford[12], J.A. Dunmore[11,21], E.D. Earle[13], H.C. Evans[13], G.T. Ewan[13], J. Farine[5], H. Fergani[11], F. Fleurot[5], R.J. Ford[16,13], J.A. Formaggio[10,15], N. Gagnon[15,7,6,11], J.TM. Goon[9], K. Graham[13], E. Guillian[13], R.L. Hahn[2], A.L. Hallin[13], E.D. Hallman[5], P.J. Harvey[13], R. Hazama[15,22], K.M. Heeger[15,6], W.J. Heintzelman[12], J. Heise[16], R.L. Helmer[18,1], R.J. Hemingway[3], R. Henning[6], A. Hime[7], C. Howard[13], M.A. Howe[15], M. Huang[17], P. Jagam[4], N.A. Jelley[11], J.R. Klein[17,12], L.L. Kormos[13], M. Kos[13], A. Krüger[5], C. Kraus[13], C.B. Krauss[13], T. Kutter[9], C.C.M. Kyba[12], H. Labranche[4], R. Lange[2], J. Law[4], I.T. Lawson[16,4], K.T. Lesko[6], J.R. Leslie[13], J.C. Loach[11], S. Luoma[5], R. MacLellan[13], S. Majerus[11], H.B. Mak[13], J. Maneira[8], A.D. Marino[6,23], R. Martin[13], N. McCauley[12,24], A.B. McDonald[13], S. McGee[15], C. Mifflin[3], K.K.S. Miknaitis[15,25], M.L. Miller[10], B. Monreal[10], B.G. Nickel[4], A.J. Noble[13], E.B. Norman[6,26], N.S. Oblath[15], C.E. Okada[6,27], H.M. O'Keeffe[11], G.D. Orebi Gann[11], S.M. Oser[1], R. Ott[10], S.J.M. Peeters[11], A.W.P. Poon[6], G. Prior[6], K. Rielage[7,15], B.C. Robertson[13], R.G.H. Robertson[15], E. Rollin[3], M.H. Schwendener[5], J.A. Secrest[12], S.R. Seibert[17], O. Simard[3], C.J. Sims[11], D. Sinclair[3,18], P. Skensved[13], R.G. Stokstad[6], L.C. Stonehill[7,15], G. Tešić[3], N. Tolich[6], T. Tsui[1], R. Van Berg[12], R.G. Van de Water[7], B.A. VanDevender[15], C.J. Virtue[5], T.J. Walker[10], B.L. Wall[15], D. Waller[3], H. Wan Chan Tseung[11], D.L. Wark[14,29], J. Wendland[1], N. West[11], J.F. Wilkerson[15], J.R. Wilson[11,28], J.M. Wouters[7], A. Wright[13], M. Yeh[2], F. Zhang[3], K. Zuber[11,28]

ABSTRACT

A search has been made for neutrinos from the *hep* reaction in the Sun and from the diffuse supernova neutrino background (DSNB) using data collected during the first operational phase of the Sudbury Neutrino Observatory, with an exposure of 0.65 kilotonne-years. For the *hep* neutrino search, two events are observed in the effective electron energy range of 14.3 MeV $< T_{eff} <$ 20 MeV where 3.1 background events are expected. After accounting for neutrino oscillations, an upper limit of 2.3×10^4 cm^{-2}s^{-1} at the 90% confidence level is inferred on the integral total flux of *hep* neutrinos. For DSNB neutrinos, no events are observed in the effective electron energy range of 21 MeV $< T_{eff} <$ 35 MeV and, consequently, an upper limit on the ν_e component of the DSNB flux in the neutrino energy range of 22.9 MeV $< E_\nu <$ 36.9 MeV of 70 cm^{-2}s^{-1} is inferred at the 90% confidence level. This is an improvement by a factor of 6.5 on the previous best upper limit on the *hep* neutrino flux and by two orders of magnitude on the previous upper limit on the ν_e component of the DSNB flux.

Subject headings: neutrinos, Sun: general, supernovae: general

[1] Department of Physics and Astronomy, University of British Columbia, Vancouver, BC V6T 1Z1, Canada

[2] Chemistry Department, Brookhaven National Laboratory, Upton, NY 11973-5000

[3] Ottawa-Carleton Institute for Physics, Department of Physics, Carleton University, Ottawa, Ontario K1S 5B6, Canada

[4] Physics Department, University of Guelph, Guelph, Ontario N1G 2W1, Canada

[5] Department of Physics and Astronomy, Laurentian University, Sudbury, Ontario P3E 2C6, Canada

[6] Institute for Nuclear and Particle Astrophysics and Nuclear Science Division, Lawrence Berkeley National Laboratory, Berkeley, CA 94720

[7] Los Alamos National Laboratory, Los Alamos, NM 87545

[8] Laboratório de Instrumentação e Física Experimenttal de Partículas, Lisboa, Portugal

[9] Department of Physics and Astronomy, Louisiana State University, Baton Rouge, LA 70803

[10] Laboratory for Nuclear Science, Massachusetts Institute of Technology, Cambridge, MA 02139

[11] Department of Physics, University of Oxford, Denys Wilkinson Building, Keble Road, Oxford OX1 3RH, UK

[12] Department of Physics and Astronomy, University of Pennsylvania, Philadelphia, PA 19104-6396

[13] Department of Physics, Queen's University, Kingston, Ontario K7L 3N6, Canada

[14] Rutherford Appleton Laboratory, Chilton, Didcot OX11 0QX, UK

[15] Center for Experimental Nuclear Physics and Astrophysics, and Department of Physics, University of Washington, Seattle, WA 98195

[16] SNOLAB, P.O. Box 146, Lively, ON P3Y 1M3, Canada

[17] Department of Physics, University of Texas at Austin, Austin, TX 78712-0264

[18] TRIUMF, 4004 Wesbrook Mall, Vancouver, BC V6T 2A3, Canada

[19] Present address: Goldman Sachs, 85 Broad Street, New York, NY

[20] Present address: Physics Department, Princeton University, Princeton, NJ 08544-0708

[21] Present address: Department of Physics, University of California, Irvine, CA

[22] Present address: Graduate School of Engineering, Hiroshima University, Hiroshima, Japan

[23] Present address: Fermilab, Batavia, IL

[24] Present address: Department of Physics, University of Liverpool, Liverpool, L69 7ZE, UK

[25] Present address: Department of Physics, University of Chicago, Chicago, IL

[26] Present address: Lawrence Livermore National Laboratory, Livermore, CA

[27] Present address: Remote Sensing Lab, P.O. Box 98521, Las Vegas, NV 89193

[28] Present address: Department of Physics and Astronomy, University of Sussex, Brighton BN1 9QH, UK

[29] Alternate address: Imperial College, London SW7 2AZ, UK

1. Introduction

The Sudbury Neutrino Observatory (SNO) is a real-time, heavy water Cherenkov detector located in the Inco, Ltd. Creighton nickel mine near Sudbury, Ontario, Canada at a depth of 6010 m water equivalent (Boger *et al.* (2000)). SNO detects electrons and neutrons from, respectively, charged-current (CC) and neutral-current (NC) interactions of neutrinos on deuterons, as well as neutrino-electron elastic scattering (ES) interactions, in one kilotonne of D_2O contained in a 12 m diameter acrylic vessel (AV). These interactions are observed via Cherenkov light detected by 9456 photomultiplier tubes (PMTs) mounted on a 17.8 m diameter support structure. By comparing the observed rates of these interactions, SNO has demonstrated that a substantial fraction of the ^{8}B electron neutrinos produced in the Sun transform into other active neutrino flavors (Ahmad *et al.* (2001, 2002a,b); Ahmed *et al.* (2004); Aharmim *et al.* (2005)). These results are consistent with the predictions of neutrino oscillations (Maki, Nakagawa & Sakata (1962); Gribov & Pontecorvo (1969); Wolfenstein (1978); Mikheyev & Smirnov (1985)).

The Sun generates energy by nuclear fusion; protons combine to form helium in reactions that release neutrinos. The primary solar fusion process is a series of reactions known as the pp chain. Five reactions in the pp chain produce neutrinos; the highest energy neutrinos are those from the *hep* reaction: $^3\mathrm{He} + \mathrm{p} \rightarrow {}^4\mathrm{He} + \mathrm{e}^+ + \nu_e$. The endpoint of the *hep* neutrino spectrum is 18.77 MeV and lies above that of the ^{8}B spectrum, which is approximately 15 MeV. The flux of *hep* neutrinos (*e.g.* Bahcall & Krastev (1998), Bachall & Pinsonneault (2004)) is currently predicted to be $(7.97 \pm 1.24) \times 10^3$ cm^{-2}s^{-1} (Bahcall, Serenelli & Basu (2005)), which is small compared to the fluxes from the other neutrino-producing reactions in the pp chain, including the ^{8}B flux which has been measured to be $(4.95 \pm 0.42) \times 10^6$ cm^{-2}s^{-1} (Aharmim *et al.* (2005)). The dominant contribution to the uncertainty in the *hep*

neutrino flux prediction is 15.1% from the calculation of the nuclear matrix elements (Park *et al.* (2003)). The previous best upper limit on the *hep* neutrino flux is 7.3×10^4 cm^{-2}s^{-1} at the 90% confidence level (CL), based on measurements with the Super-Kamiokande detector (Hosaka *et al.* (2005)). After accounting for neutrino oscillations, this limit can be interpreted as an upper bound on the total flux of *hep* neutrinos of 1.5×10^5 cm^{-2}s^{-1}. Currently, only one reaction (^{8}B) from the pp chain has been uniquely observed and measured experimentally. An observation of *hep* neutrinos would give further confirmation of the pp chain as the primary solar energy generation mechanism and would allow further tests of the solar model.

Neutrinos produced in core-collapse supernovae also contribute to the energy region above the ^{8}B endpoint. The current generation of neutrino detectors can detect the transient signal from a supernova in the Milky Way, but the expected signal from a supernova in a more distant galaxy is fewer than one event. Neutrinos from all extragalactic supernovae since the beginning of the formation of stars in the universe constitute the diffuse supernova neutrino background (DSNB), which may be detectable. Model predictions range from 0.19 to 1.49 cm^{-2}s^{-1} for the ν_e component of the DSNB flux in the neutrino energy range 22.9 MeV $< E_\nu <$ 36.9 MeV (Beacom & Strigari (2006), Ando & Sato (2003)). The best upper limit on the $\overline{\nu}_e$ component of the DSNB flux is 1.2 cm^{-2}s^{-1} at the 90% CL for $E_{\overline{\nu}} >$ 19.3 MeV, based on measurements with the Super-Kamiokande detector (Malek *et al.* (2003)). While an indirect limit on the ν_e component of the DSNB flux can be inferred from this (Lunardini (2006)), the previous best direct upper limit is 6.8×10^3 cm^{-2}s^{-1} for neutrino energies 25 MeV $< E_\nu <$ 50 MeV, based on measurements with the Mont Blanc liquid scintillator detector (Aglietta *et al.* (1992)).

A search for *hep* and DSNB neutrinos has been performed by counting the numbers of events in predefined energy intervals (signal boxes) above the ^{8}B endpoint. The most sensitive signal boxes for this analysis were selected by evaluating the predicted signal and background levels before examining the data. Given the predicted signal and background levels in the signal boxes, limits on the flux of *hep* and DSNB neutrinos are set using a modified Feldman-Cousins technique. The following sections describe the data set, detector response, determination of the backgrounds, analysis procedures and the limits obtained for the *hep* and DSNB neutrino fluxes.

2. The Data Set

The data included in these analyses were collected during the initial phase of SNO operation, during which the detector contained pure D_2O. The data were collected from 1999 November 2 until 2001 May 28 and comprise 306.4 live days corresponding to an exposure of 0.65 kilotonne-years (Ahmad *et al.* (2002a)).

Since results from this phase were last published, numerous improvements have been made to the analysis tools, many of which were used in the analysis of data from phase two (Aharmim *et al.* (2005)), for which two tonnes of salt were dissolved in the heavy water. Further improvements were applied in this analysis, the most significant of which was improved estimation of the effective electron kinetic energies ($T_{\rm eff}$) of the events, based on the optical paths to each operational PMT. Other enhancements include improved handling of false hits due to cross-talk between electronics channels and an improved accounting of working PMTs using both neutrino and calibration data to track bad channels. However, the vertex reconstruction algorithm was the same as that used in previous phase one analyses, in which events were reconstructed under the assumption that they are due to single electrons. This is more suited for the reconstruction of *hep* and DSNB events than the algorithm used in phase two. After the application of the new analysis tools, events inside the kinetic energy window of 12 MeV $< T_{\rm eff} <$ 35 MeV were not examined until the *hep* and DSNB signal boxes had been selected.

In addition to the event selection discussed in Aharmim *et al.* (2005), which includes a selection that removes Michel electrons with visible precursors, selection criteria were applied to remove backgrounds from atmospheric neutrino interactions. As the *hep* and DSNB signals are expected to be single electron events, these backgrounds can be reduced significantly by removing events which correlate in time with neutrons, electrons or γ-rays. Consequently, any candidate

event that appeared within 250 ms of another with $T_{eff} > 4$ MeV and a reconstructed vertex inside the AV was removed. In addition, two Kolmogorov-Smirnov (KS) tests were applied: one to test the azimuthal symmetry of the PMT hits about the reconstructed event direction; the other to test the compatibility of the angular distribution of PMT hits with that expected from a single electron. In the signal boxes, the selections on PMT hit isotropy and the prompt light fraction were further tightened with respect to previous SNO analyses (Aharmim *et al.* (2005)). This was possible in this analysis due to the higher energies of the candidate events. The combined event selection reduced the expected number of atmospheric neutrino events in the *hep* signal box by a factor of 29 and by a factor of 77 in the DSNB signal box. The signal acceptance of the combined event selection is $(96.6 \pm 0.7)\%$ for *hep* and $(94.0 \pm 1.5)\%$ for DSNB events, measured using calibration source data and simulation.

3. Detector Response

To understand the signals and backgrounds in this analysis, it is important to measure the energy response and uncertainties in the signal boxes. The energy response can be parameterized by a Gaussian of resolution $\sigma_T = -0.154 + 0.390\sqrt{T_e} + 0.0336T_e$, where T_e is the true kinetic energy of the electron. In SNO analyses, Monte Carlo simulation is used to estimate the response of the detector to different particles. The propagation of electrons, positrons and γ-rays is carried out using EGS4 (Nelson, Hirayama & Rogers (1985)). The uncertainties in the energy scale and resolution of the SNO detector have typically been measured using 6.13 MeV γ-rays from a ^{16}N source (Dragowsky *et al.* (2001)). At the higher energies more characteristic of this analysis, Michel electrons from muon decays and a pT (^{3}H(p,γ)^{4}He) source (Poon *et al.* (2000)), which produces 19.8 MeV γ-rays, were used to complement the ^{16}N measurements. Using simple event selection criteria, including one based on the time between events, 135 Michel electrons were identified in the data. Potential deviations in energy scale and energy resolution between data and simulations were assumed to be linear functions of energy. These functions were fit with a maximum likelihood technique using data from ^{16}N and pT sources as further constraints. The results were used to refine the energy scale and resolution estimates and to measure their uncertainties at the analysis thresholds. An energy scale uncertainty of 0.96% and a resolution uncertainty of 3.8% were estimated at the *hep* threshold of 14.3 MeV. At the DSNB threshold of 21 MeV, an energy scale uncertainty of 1.06% and a resolution uncertainty of 6.0% were estimated. Correlations between these quantities were included in the final analysis. Additional non-Gaussian tails to the resolution function were also considered, but were found to be insignificant. Data and Monte Carlo distributions of T_{eff} for ^{16}N and pT calibration events and for Michel electrons are shown in Figure 1.

Event vertex and direction reconstruction were unchanged from the analysis in Ahmad *et al.* (2002a). The position resolution at 15 MeV is (12.0 ± 2.5) cm and the angular resolution is $(20.6 \pm 0.4)^{\circ}$. These were measured using a combination of ^{16}N source data and simulation. The same fiducial volume, defined by events reconstructed within a distance of 550 cm from the center of the detector, was selected. The uncertainty on the expected number of events within the fiducial volume due to vertex accuracy was 2.9%.

4. Backgrounds

Three distinct classes of background are considered: ^{8}B neutrino interactions, atmospheric neutrino interactions and instrumental backgrounds. Figure 2 shows the simulated energy spectra of the signals and backgrounds, normalized to their expected rates.

Electrons from ^{8}B neutrino interactions are the dominant (97%) background for the *hep* analysis but are a negligible background for DSNB. These events can reconstruct into the *hep* signal box due to the finite energy resolution of the detector. The magnitude of the ^{8}B background depends on the details of the detector response and is very sensitive to the energy scale and resolution at threshold. In the CC interaction, by which SNO predominantly detects the ^{8}B and *hep* neutrinos, there is a strong correlation between neutrino and electron energy. This, in addition to a cross section that rises with the square of the energy rather than linearly, provides a clearer distinction between the two neutrino spectra in the region of the ^{8}B end-

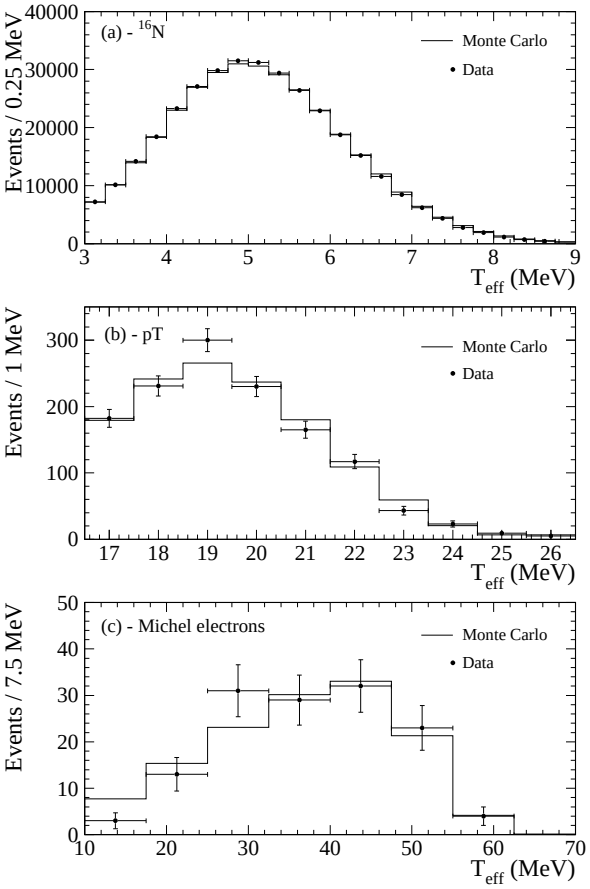

Fig. 1.— The effective electron kinetic energy spectra from data and Monte Carlo for (a) events from the ^{16}N source, (b) events from the pT source and (c) Michel electrons. The data are shown in the energy regions free of source related backgrounds.

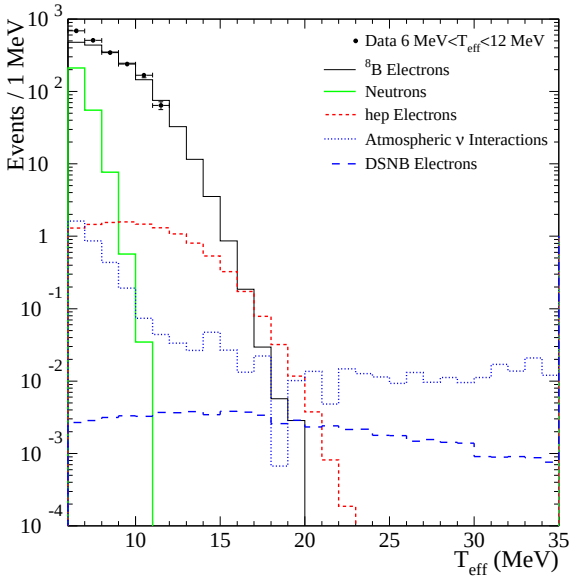

Fig. 2.— The simulated effective electron kinetic energy spectra of the signals and backgrounds of interest in the *hep* and DSNB analyses. Also shown are the data in the range 6 MeV < T_{eff} < 12 MeV which are used to normalize the ^{8}B electron and neutron distributions. The atmospheric neutrino background is made up of a number of different signals: neutrons at low energies; γ-rays from nuclear de-excitations at intermediate energies; and Michel electrons and CC interactions of atmospheric ν_e and $\bar{\nu_e}$ on deuterons at higher energies. The DSNB model in this figure is the $T = 6$ MeV model from Beacom & Strigari (2006). The third class of background, instrumental backgrounds, which is not shown in this figure is negligible.

point than is possible with the ES interaction.

The ^{8}B background also depends on the details of the shape of the detected electron spectrum. The ^{8}B neutrino spectrum from Winter *et al.* (2003, 2006) was assumed along with its quoted uncertainties. Neutrino oscillations were taken into account by correcting and combining the electron spectra from CC and ES interactions using the energy-dependent ν_e survival probability from the joint solar neutrino and KamLAND (Araki *et al.* (2005)) oscillation analysis presented in Aharmim *et al.* (2005). Additional spectral adjustments were included to account for CC interactions on ^{18}O, radiative corrections to the CC deuteron cross section (Nakamura *et al.* (2002); Kurylov *et al.* (2002)) and the acceptance of the event selection. The expectation for the hep signal is constructed in the same way using the neutrino spectrum from Bahcall & Ulrich (1988) with corrections from Bahcall (1997).

After the determination of the ^{8}B signal shape, its normalization was determined using data at lower energies, where the *hep* signal is insignificant. In an energy window of 6 MeV $< T_{\rm eff} <$ 12 MeV, 2006 events were observed. To determine normalizations, these data were fit using a maximum likelihood technique with probability density functions (PDFs) for the ^{8}B electrons (CC and ES signals) and neutrons (NC signal and background). The distributions used in this fit were functions of event energy and direction with respect to the Sun ($\cos\theta_\odot$). The results of this fit were then used to estimate the ^{8}B contribution inside the signal boxes.

Atmospheric neutrino interactions produce a second class of background events. They are the dominant background in the DSNB signal box and come from several sources:

- Electrons from low energy ($E_\nu < 100$ MeV) charged-current ν_e and $\overline{\nu}_e$ interactions;
- Michel electron events, where the precursor muons (and pions) are below the Cherenkov threshold and do not trigger the detector;
- 15.1 MeV γ-rays from de-excitation of an excited state of ^{12}C created via a nuclear cascade from neutrino interactions on ^{16}O;
- Mis-identified non-electron events.

For low energy atmospheric ν_e and $\overline{\nu}_e$, the flux prediction from Battistoni *et al.* (2005) is used, which has an uncertainty of 25%. Only charged current interactions on deuterons, with cross sections from Nakamura *et al.* (2002) and Kurylov *et al.* (2002) are considered; the contributions from other interaction types are not significant. The interactions of these neutrinos constitute 14% of the DSNB background, but are insignificant in the *hep* signal box.

Events from the latter three sources are associated with atmospheric neutrinos of higher energy ($E_\nu > 100$ MeV). Monte Carlo simulations were used to generate atmospheric neutrino interactions in the SNO detector with statistics equivalent to 500 times the expected number of events. For this purpose, the package NUANCE (Casper (2002)) was used, with the Bartol04 flux prediction for Sudbury (Barr *et al.* (2004)). The flux uncertainty in the neutrino energy range that contributes to the background is 10%. The events generated by NUANCE were then propagated and fully simulated in the SNO Monte Carlo, from which background predictions were obtained after application of the event selection.

To assess uncertainties these events were divided into three categories. The first category, ν_μ quasi-elastic (QE) CC events, is the primary source of untagged Michel electrons and originates from neutrinos in the energy range 150 to 250 MeV. The uncertainty on the cross section in this energy region is 25% (Barish *et al.* (1977)). These Michel electrons comprise 80% of the DSNB background. For the second category, 15.1 MeV γ-ray events, there is no data in the literature on production rates and, thus, a 100% uncertainty was assigned to the production rate predicted by NUANCE, which uses the calculation of Ejiri (1993). These γ-rays constitute half of the atmospheric background in the *hep* analysis, but due to the magnitude of the ^{8}B background constitute only 1.5% of the total *hep* background. The final category comprises QE NC events and interactions that produce pions, to which a cross section uncertainty of 30% is assigned (Ahrens *et al.* (1987)).

There is an additional uncertainty applicable to the latter two categories of atmospheric neutrino interactions. A comparison of events from data and the simulation has shown that the simulation underestimates the production of correlated neu-

trons. It is unclear if this is due to errors in the prediction of primary neutron production or in the transport of hadrons in the simulation. However, there is good agreement between data and Monte Carlo for correlated electron events. Events in the simulation are re-weighted in such a way that the average neutron multiplicity is changed to better match the data. This results in a change to the background rejection rate in the simulation due to time correlated neutrons. This correction results in an additional uncertainty of 7% in the rate of atmospheric background events inside the signal box that are not due to QE CC interactions. After application of the event selection to remove events with correlated neutrons, electrons and gamma-rays the atmospheric background in these analyses is reduced by a factor of two.

To verify the predictions for the atmospheric neutrino background, data outside the signal box in the energy range 35 MeV $< T_{eff} <$ 55 MeV were examined. This energy range was selected to be most sensitive to the main component of the atmospheric neutrino background: the Michel electrons. In this energy range, 0.28 Michel electrons and 0.05 electrons from low energy charged-current atmospheric neutrino interactions are expected. One event was observed, consistent with the predictions of the simulation. Inside this energy range, the effect of the event selection on events correlated with neutrons, electrons or γ-rays was also examined. Two such events were observed, each consistent with being an otherwise untagged Michel electron preceded by a γ-ray from the de-excitation of the nucleus participating in the primary neutrino interaction. No events were observed that are correlated with neutron or electron events. These results are also consistent with the predictions of the simulation.

The final class of backgrounds is associated with instrumental effects such as electronic pickup or static discharge from the PMTs. For these events, an upper limit of 0.002 events is set in an energy range of 6 MeV $< T_{eff} <$ 35 MeV using the technique described in Aharmim *et al.* (2005). This analysis is not sensitive to the isotropic acrylic vessel background (IAVB) (see Aharmim *et al.* (2005)). To predict the number of IAVB events that pass the signal event selection, the 13 IAVB events clearly identified in the data by simple criteria are scaled via Monte Carlo simulation. A limit of 7×10^{-4} IAVB events in the energy range of 14 MeV $< T_{eff} <$ 35 MeV is inferred at the 90% CL.

5. Analysis and results

The analysis was designed to construct confidence intervals on the neutrino fluxes using a modified Feldman-Cousins approach (Cousins & Feldman (1998); Conrad *et al.* (2003); Hill (2003)). Limits were also calculated using a Bayesian approach (Eidelman *et al.* (2004)); very similar results are obtained for the two techniques. To determine confidence limits the probability $p(N|S)$ of observing N events, given a signal flux S, is calculated taking statistical fluctuations and all known systematic uncertainties into account. A Monte Carlo technique is used to integrate over the estimated distributions of the systematic uncertainties, including known correlations, by sampling ensembles of shifted parameter values and propagating their effect on the PDFs and extracted signal and background normalizations. The major uncertainties included in this procedure are shown in Table 1.

The *hep* and DSNB analyses are very similar, except that the definitions of signal and background are modified. In the DSNB analysis, the *hep* distribution is scaled using the standard solar model prediction, including its uncertainty, and added to the background estimate.

For the *hep* analysis the signal box was chosen to optimize the sensitivity based on Monte Carlo simulations. The sensitivity was defined as the mean value, from an ensemble of Monte Carlo experiments, of the 90% CL upper limit for the *hep* flux, integrated over all energies using the *hep* neutrino spectrum and accounting for neutrino oscillations as discussed in Section 4, assuming the standard solar model. Figure 3a shows the predicted numbers of signal and background events with their 1σ uncertainties as the lower threshold of the *hep* signal box is changed, and Figure 3b shows the sensitivity of the analysis as a function of the signal box threshold. There is a region between 12.5 MeV and 14.3 MeV where the sensitivity is nearly flat. Within this range the choice of the best signal box is a compromise between the signal to background ratio and signal acceptance. The energy range 14.3 MeV $< T_{eff} <$ 20 MeV was

Table 1: Major uncertainties included in the analyses.

Source of Uncertainty	Magnitude of effect
Energy scale	
T_{eff} = 14.3 MeV	0.96%
T_{eff} = 21 MeV	1.06%
Energy resolution	
T_{eff} = 14.3 MeV	3.8%
T_{eff} = 21 MeV	6.0%
Vertex accuracy	2.9%
Vertex resolution	2.5 cm
Angular resolution	2%
^{8}B ν_e spectrum	Taken from 1
$\tan^2(\theta_{12})$, Δm^2_{12}	Contours from 2
ν_{atm} flux	
$E_\nu > 100$ MeV	10%
$E_\nu < 100$ MeV	25%
Cross sections	
CC deuteron	1.2%
ν_{atm} CC QE	25%
ν_{atm} other	30%
15.1 MeV γ-rays	100%
ν_{atm} n-multiplicity	7%

References. — (1) Winter *et al.* (2006); (2) Aharmim *et al.* (2005)

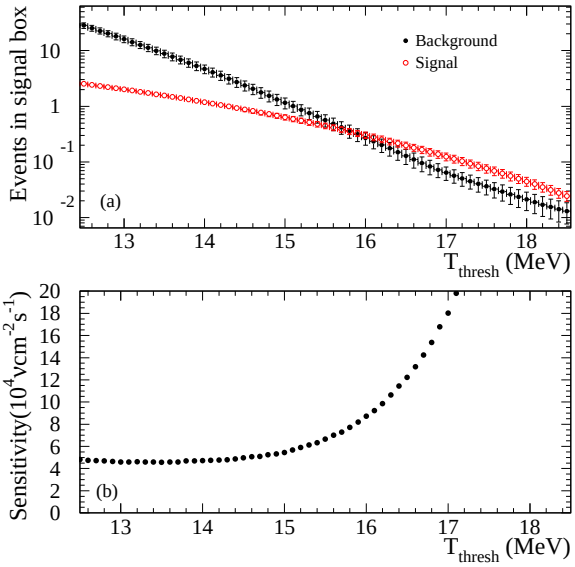

Fig. 3.— Panels (a) and (b) show the expected number of events and the sensitivity of the analysis respectively as the energy threshold of the *hep* signal box is varied. The hep flux in panel (a) is normalized to the solar model prediction. The upper limit of the signal box is fixed at 20 MeV.

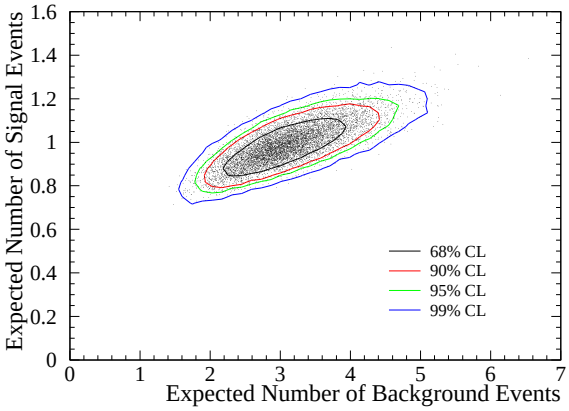

Fig. 4.— The joint probability distribution of signal and background events in the *hep* signal box assuming the standard solar model flux of *hep* neutrinos.

selected. In this range, the variations of predicted signal and background levels due to systematic uncertainties are strongly correlated, as can be seen in Figure 4. In this signal box, 3.13 ± 0.60 background events and 0.99 ± 0.09 signal events are expected. The contributions to the signal and background uncertainties from the dominant sources of systematic uncertainties are shown in Table 2.

Two events are observed in the *hep* signal box. After accounting for the effect of neutrino oscillations, this results in an upper limit on the integral total *hep* neutrino flux of 2.3×10^4 cm^{-2}s^{-1} at the 90% CL. This is 2.9 times the prediction of the standard solar model. Using a Bayesian technique rather than the modified Feldman-Cousins approach, a limit of 2.9×10^4 cm^{-2}s^{-1} is found at the 90% CL. The spectrum of events in the region of the signal box is shown in Figure 5. The shape agrees with the background prediction at the 77.8% CL based on Monte Carlo simulations

Table 2: The effect of systematics on *hep* signal and background

Systematic Source	ΔBkg(%)	ΔSig(%)
Energy scale	13.7	7.6
Energy resolution	9.7	0.7
Vertex accuracy	0.3	2.9
^{8}B ν_e spectrum	0.8	0.0
ν_{atm} flux	0.3	0.0
Δm^2_{12}	0.6	0.5
$\tan^2(\theta_{12})$	0.7	3.2
Cross sections		
CC deuteron	0.0	1.1
ν_{atm} CC QE	0.3	0.0
15.1 MeV γ-rays	0.8	0.0
Low energy fit statistics	3.1	0.0
Combined Width	19.1	9.0

NOTE.—This table shows the one standard deviation contributions to the width of the signal (ΔSig) and background (ΔBkg) probability distributions in the *hep* signal box. The combined widths are greater than the quadrature sums of the systematics due to correlations and non-linearities.

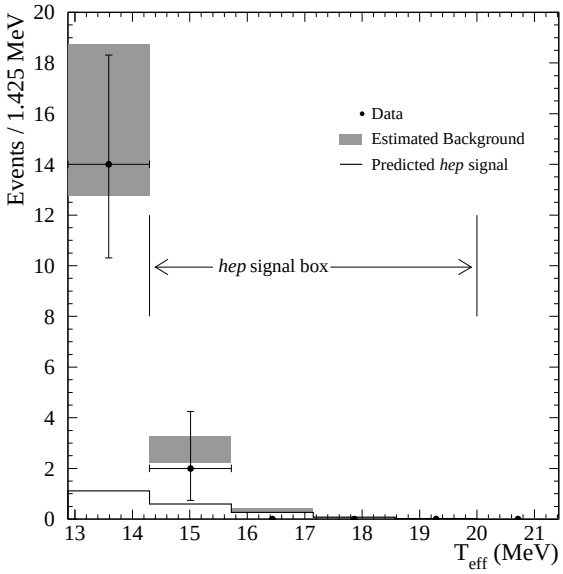

Fig. 5.— The distribution of events in the region of the ^{8}B endpoint. There are two events in the *hep* signal box 14.3 MeV $< T_{eff} <$ 20 MeV. Also shown are the estimated number of background events, including the systematic uncertainty, and the standard solar model prediction for the *hep* signal.

using a KS statistic.

This result is model-dependent, as neutrino oscillations were assumed in the predictions of signal and background. A model-independent search, in which a limit is placed on the ν_e component of the integral *hep* flux, was also carried out. This search is independent of any model of neutrino flavor change. A further event selection of $\cos\theta_\odot < 0.8$ was applied to remove ES events (which are directed away from the Sun) and leave events due only to CC (ν_e) interactions. The energy threshold was selected so that the mean background expectation was less than 0.25 events, and flux limits were set conservatively by assuming there is no background and quoting only the upper bound. With these criteria, a signal box of 16 MeV $< T_{eff} <$ 20 MeV was selected. Without neutrino oscillations 0.66 ± 0.08 *hep* events are expected in this box. As no events are observed a limit on the ν_e component of the integral *hep* neutrino flux of 3.1×10^4 cm^{-2}s^{-1} at the 90% CL is inferred.

Signal box selection for the DSNB search follows the approach of the *hep* neutrino search. A signal box of 21 MeV $< T_{eff} <$ 35 MeV was selected in this case. This choice was bounded at the high end by the prior choice of the hidden energy interval and at the low end by a desire to minimize any contribution from *hep* neutrinos. In this signal box, 0.18 ± 0.04 background events are expected. The expected number of signal events depends upon the assumed DSNB model, but is uncorrelated with the background prediction as different systematic uncertainties are dominant for signal and background. The estimated values of the systematic uncertainties are shown in Table 3. No events are observed in the signal box, resulting in an upper limit of 2.3 events due to DSNB neutrinos at the 90% CL.

To obtain a DSNB flux limit, a spectral model for the DSNB neutrinos is required. In this paper, three models from Beacom & Strigari (2006) and two models from Ando & Sato (2003) for differential flux predictions have been used. Table 4 shows

Table 3: The effect of systematics on DSNB signal and background

Systematic Source	ΔBkg(%)	ΔSig(%)
Energy scale	3.4	0.9
Energy resolution	1.7	0.4
Vertex accuracy	2.9	2.9
Event selection	0.9	1.7
ν fluxes		
ν_{atm} $E_\nu > 100$ MeV	8.6	0.0
ν_{atm} $E_\nu < 100$ MeV	3.5	0.0
hep	0.2	0.0
Cross sections		
ν_{atm} CC QE	19.2	0.0
ν_{atm} other	2.6	0.0
CC deuteron	0.2	1.2
ν_{atm} n-multiplicity	0.7	0.0
Combined Width	24.7	4.3

NOTE.—This table shows the one standard deviation contributions to the width of the signal (ΔSig) and background (ΔBkg) distributions in the DSNB signal boxes. For the DSNB signal the $T = 6$ MeV model from Beacom & Strigari (2006) is used. As in the prediction for the signal and background in the *hep* signal box, combined widths are greater than the quadrature sums of the systematics.

the integral flux predictions for these models and the 90% CL upper limits inferred from data.

Using these results, a limit can also be derived on the DSNB ν_e flux for neutrinos that produce electrons with kinetic energies inside the DSNB signal box. Although the integral flux upper limits are significantly different for these models, since their spectral shapes are similar in the signal box, the resulting upper limits for the neutrinos in this region vary little (see Table 4). Taking the median result a limit on the DSNB ν_e flux of 70 $\mathrm{cm^{-2}s^{-1}}$ at the 90% CL for 22.9 MeV $< E_\nu <$ 36.9 MeV is inferred. These limits and the background prediction are in good agreement with those predicted by Beacom & Strigari (2006), after accounting for the difference in exposure between their prediction and the data used in this search.

6. Conclusions

Data from the first operational phase of SNO, with an exposure of 0.65 kilotonne-years, have been used to search for neutrinos from the *hep* reaction in the Sun. No evidence for these neutrinos was observed, and an upper limit on the integral total flux of *hep* neutrinos of 2.3×10^4 $\mathrm{cm^{-2}s^{-1}}$ has been derived at the 90% CL. This measurement improves the previous best limit on the *hep* neutrino flux, measured with the Super-Kamiokande detector, by a factor of 6.5, but is not inconsistent with the standard solar model. A model-independent limit on the integral *hep* ν_e flux, with no assumptions about neutrino oscillations, is set at 3.1×10^4 $\mathrm{cm^{-2}s^{-1}}$. A search for the ν_e component of the diffuse supernova neutrino background has also been made using SNO data. Again, no evidence for these neutrinos was found, and an upper limit at 90% CL on the ν_e component of the DSNB flux of 70 $\mathrm{cm^{-2}s^{-1}}$ for 22.9 MeV $< E_\nu <$ 36.9 MeV is inferred. This is an improvement of two orders of magnitude on the previous ν_e limit (Aglietta *et al.* (1992)). The exposure of the final SNO data set for these analyses combined across all phases of the experiment, is expected to be approximately four times that of the data used in this analysis. A future search for *hep* and DSNB fluxes using these data will be carried out, which is expected to further improve upon the limits presented in this paper.

This research was supported by: Canada: Natural Sciences and Engineering Research Council, Industry Canada, National Research Council, Northern Ontario Heritage Fund, Atomic Energy of Canada, Ltd., Ontario Power Generation, High Performance Computing Virtual Laboratory, Canada Foundation for Innovation; US: Department of Energy, National Energy Research Scientific Computing Center, Alfred P. Sloan Foundation; UK: Particle Physics and Astronomy Research Council. We thank the SNO technical staff for their strong contributions. We thank Inco, Ltd. for hosting this project.

REFERENCES

Aglietta M *et al.* 1992, Astropart. Phys. **1**, 1.

Aharmim B. *et al.* 2005, Phys. Rev. C **72**, 055502.

Ahmad Q.R. *et al.* 2001, Phys. Rev. Lett. **87**, 071301.

Ahmad Q.R. *et al.* 2002, Phys. Rev. Lett. **89**, 011301.

Ahmad Q.R. *et al.* 2002, Phys. Rev. Lett. **89**, 011302.

Ahmed S.N. *et al.* 2004, Phys. Rev. Lett. **92**, 181301.

Ahrens L.A. *et al.* 1987, Phys. Rev. D **35**, 785.

Ando S. & Sato K. 2003, Phys. Lett. B **559**, 113. Flux predictions from this paper have been increased by a factor of three, as recommended by the authors, to account for updated star formation rate data. Estimates for the ν_e DSNB fluxes were provided by the authors upon request.

Araki T. *et al.*, 2005 Phys. Rev. Lett. **94**, 081801.

Bahcall J.N. 1997, Phys. Rev. C **56**, 3391.

Bahcall J.N. & Krastev P.I 1998, Phys. Lett. B **436**, 243.

Bahcall J.N & Pinsonneault M.H. 2004, Phys. Rev. Lett. **92**, 121301.

Bahcall J.N., Serenelli A.M. & Basu S. 2005, preprint (astro-ph/0511337v1). The GS98 elemental abundances are selected for reference model of solar neutrino fluxes.

Bahcall J.N. & Ulrich R.K. 1988, Rev. Mod. Phys. **60**, 297.

Barish S.J. *et al.* 1977, Phys. Rev. D **16**, 3103.

Barr G.D *et al.* 2004, Phys. Rev. D **70**, 023006.

Battistoni G. *et al.* 2005, Astropart. Phys. **23**, 526.

Beacom J.F. & Strigari L.F. 2006, Phys. Rev. C **73**, 035807.

Boger J. *et al.* 2000, Nucl. Instr. and Meth. A **449**, 172.

Casper D. 2002, Nucl. Phys. Proc. Suppl. **112**, 161. NUANCE version 3r009 was used in this analysis.

Conrad J. *et al.* 2003, Phys. Rev. D **67**, 012002.

Cousins R.D. & Feldman G.J. 1998, Phys. Rev. D **57**, 3873.

Dragowsky M.R. *et al.* 2001, Nucl. Instr and .Meth. A **481**, 284.

Eidelman S. *et al.* 2004, Phys. Lett. B **592**, 1

Ejiri H. 1993, Phys. Rev. C **48**, 1442-1444.

Gribov V. & Pontecorvo B. 1969, Phys. Lett. B. **28**, 493.

Hill G.C. 2003, Phys. Rev. D **67**, 118101.

Hosaka J *et al.* 2006, Phys. Rev. D **73**, 112001.

Kurylov A *et al.* 2002, Phys. Rev. C **65**, 055501.

Lunardini C. 2006, Phys. Rev. D **73**, 083009.

Malek M *et al.* 2003, Phys. Rev. Lett. **90**, 071301.

Mikheyev S.P. & Smirnov A.Yu. 1985 Sov. J. Nucl. Phys. **42**, 913.

Maki Z., Nakagawa N. & Sakata S. 1962, Prog. Theor. Phys. **28**, 870.

Nakamura S. *et al.* 2002, Nucl. Phys. A **707**, 561-576.

Nelson W.O., Hirayama H. & Rogers D.W.O 1985, SLAC Report 265.

Park T.S. *et al.* 2003, Phys. Rev. C **67**, 055206.

Poon A.W.P. *et al.* 2000, Nucl. Instr. Meth. A, **452**, 115.

Winter W.T *et al.* 2003, Phys. Rev. Lett. **91**, 252501.

Winter W.T *et al.* 2006, Phys. Rev. C **73**, 025503.

Wolfenstein L. 1978, Phys. Rev. D **17**, 2369.

This 2-column preprint was prepared with the AAS LaTeX macros v5.2.

Table 4: DSNB flux predictions and limits

	Integral Flux ($cm^{-2}s^{-1}$)		Flux 22.9 MeV $< E_\nu <$ 36.9 MeV ($cm^{-2}s^{-1}$)	
Model	Prediction	Upper Limit	Prediction	Upper Limit
B&S : $T = 4$ MeV	21.1	1.1×10^4	0.19	93
B&S : $T = 6$ MeV	14.1	1.5×10^3	0.66	72
B&S : $T = 8$ MeV	10.5	6.0×10^2	1.08	61
A&S : NOR-L	28.5	1.3×10^3	1.49	69
A&S : NOR-S-INV	34.9	2.3×10^3	1.06	70

NOTE.—This table shows the 90% CL upper limits on the ν_e component of the DSNB flux and model predictions for different models from Beacom & Strigari (2006) (B&S) and Ando & Sato (2003) (A&S).